Journal of Statistical Physics, Vol. 68, Nos. 3/4, 1992

Magnetohydrodynamics Computations with Lattice Gas Automata

Shiyi Chen,[1,2] Daniel O. Martínez,[1] W. H. Matthaeus,[1] and Hudong Chen[3]

Lattice gas automata have received considerable interest for the last several years and possibly may become a powerful numerical method for solving various partial differential equations and modeling different physical phenomena, because of their discrete and parallel nature and the capability of handling complicated boundaries. In this paper, we present recent studies on the lattice gas model for magnetohydrodynamics. The FHP-type lattice gas model has been extended to include a bidirectional random walk process, which allows well-defined statistical quantities, such as velocity and magnetic field, to be computed from the microscopic particle representation. The model incorporates a new sequential particle collision method to increase the range of useful Reynolds numbers in the model, an improvement that may also be of use in other lattice gas models. In the context of a Chapman–Enskog expansion, the model approximates the incompressible magnetic hydrodynamic equations in the limit of low Mach number and high β. Simulation results presented here demonstrate the validity of the model for several basic problems, including sound wave and Alfvén wave propagation, and diffusive Kolmogoroff-type flows.

KEY WORDS: Lattice gas; magnetohydrodynamics; Alfvén waves.

1. INTRODUCTION

Since the invention of lattice gas automata,[1,2] lattice gas methods have been used as a numerical scheme to solve the Navier–Stokes equations and other partial differential equations and as a discrete modeling approach to various physical problems. The success of lattice gas methods[3–9] from the computational point of view comes from their discrete nature, which allows their implementations to be purely parallel, local, and based almost

[1] Bartol Research Institute, University of Delaware, Newark, Delaware 19716.
[2] CNLS, MS-B258, Los Alamos National Laboratory, Los Alamos, New Mexico 87545.
[3] Department of Physics, Dartmouth College, Hanover, New Hampshire 03755.

0022-4715/92/0800-0533$06.50/0

exclusively on fast logical operations. This structure is ideal for modern parallel computers, such as the Connection Machine.[10] In addition, lattice gases are many-body dynamical systems that connect the microscopic particle picture to macroscopic physical behavior. One of the most important advantages of the lattice gas methods over other traditional approaches is that the former does not need to solve directly the physical equations, most of which are usually nonlinear partial differential equations that are not easily solved. In recent lattice gas research, the program has typically been that one designs a set of microscopic particle "collision" and "streaming" rules, defines a set of statistical operations to extract macroscopic quantities of physical importance, and then demonstrates the validity of the model either analytically or by application to specific physical problems of interest.

The basic two-dimensional lattice gas model proposed by Frisch, Hasslacher, and Pomeau (FHP)[1] consists of identical unit-mass particles on a hexagonal lattice. There are only six possible states at each cell along the links. An exclusion rule is imposed for particle occupation so that no more than one particle at a given site can have the same momentum. The two operations for particles on a lattice are collision and streaming. For modeling the incompressible Navier–Stokes equations, the collision step usually requires conservation of mass and momentum.

The extension of the basic FHP lattice gas model to simulate magnetohydrodynamics (MHD) in two dimensions was made first by Montgomery and Doolen[11,12] by considering the vector potential (a scalar quantity in two dimensions) to be the fundamental variable. In addition to the basic lattice gas model, they assigned the magnetic quantum $\sigma = 1, -1,$ or 0 to each particle. This scheme is appealing intuitively, but requires some interactions between the space-averaged variables and lattice quantities in the collision step and thus lacks of the parallel feature usually sought in lattice gas models. Another MHD lattice gas model, a purely local one, has been proposed by Chen *et al.*,[13,14] which introduces the idea of tensor lattice particles and allows the particles to have a "bidirectional" streaming.

In this paper, we will present some further theoretical results for the latter model, discuss the detailed implementation of the numerical simulations, and show some computational results for several basic MHD problems. A major extension of the original model is the use of a "sequential collision" method that permits all allowable scattering events to be detected and computed at each cell and at each time step, without the use of unrealistically large collision lookup tables. The computational results presented here are intended to address several basic questions concerning the behavior of the model, and serve to demonstrate that the basic physics

of MHD can be recovered from the lattice gas dynamics. Some limitations of the model are also addressed. The paper is organized as follows: In Section 2, we present the lattice gas model for MHD. Particles with the bidirectional random walk property are introduced here. Section 3 discusses the transport theory, where we describe our new implementation of the collision operations that serves to increase the Reynolds number. We also give the comparisons of theoretical results and numerical simulations for the kinematic viscosity and the magnetic resistivity. In Section 4, we describe Alfvén wave and linear sound wave propagation in the MHD lattice gas. A brief summary is given in the last section. Based on the results shown here, we suggest that the MHD lattice gas model may be applied with some success to more complicated physical problems, a topic that will be addressed further in subsequent reports.

2. LATTICE GAS MODEL FOR MHD

The incompressible MHD equations are described by the partial differential equations

$$\begin{aligned} \partial_t \mathbf{v} + \mathbf{v}\cdot\nabla\mathbf{v} &= -\nabla p + (\nabla\times\mathbf{B})\times\mathbf{B} + \nu\nabla^2\mathbf{v} \\ \partial_t \mathbf{B} + \mathbf{v}\cdot\nabla\mathbf{B} &= \mathbf{B}\cdot\nabla\mathbf{v} + \mu\nabla^2\mathbf{B} \\ \nabla\cdot\mathbf{v} &= \nabla\cdot\mathbf{B} = 0 \end{aligned} \tag{1}$$

where $\mathbf{v}$ and $\mathbf{B}$ are the velocity and magnetic field, respectively, in an appropriate set of units. The constant parameters ν and μ are the kinematic viscosity and the resistivity (or magnetic diffusivity). The magnetic vector potential $\mathbf{A}$ is related to $\mathbf{B}$ by $\nabla\times\mathbf{A} = \mathbf{B}$. The magnetic field modifies the motion of the fluid in the momentum equation through the Lorentz force $(\nabla\times\mathbf{B})\times\mathbf{B}$. In two dimensions, $\mathbf{v}$ and $\mathbf{B}$ lie in the x–y space and depend only on those coordinates, and, in terms of the magnetic potential $\mathbf{A} = A(x, y)\mathbf{z}$, the induction equation can be replaced by the scalar equation

$$\partial_t A + \mathbf{v}\cdot\nabla A = \mu\nabla^2 A \tag{2}$$

Equation (2) is the basic equation addressed in the model of Montgomery and Doolen.[11,12]

In order to use the lattice gas scheme to model the MHD equations, one has to consider the additional variable $\mathbf{B}$, which necessitates the introduction of additional degrees of freedom at the lattice gas level. That is, one must define an additional property of the particles. In the original FHP model, the particles can be in any one of the six momentum states which point to the nearest neighbors. Then the particle states are completely determined by one vector quantum, the momentum. In contrast, in the model of Chen *et al.*[13,14] a new kind of particle is introduced, the

tensor particle. There each particle is represented by two vectors, $\mathbf{e}_a$ and $\mathbf{e}_b$ ($a, b = 1,..., 6$). The a direction can be thought of as the usual FHP-type momentum state, specifying the velocity field, while the new direction b is directly related to the magnetic field. Therefore, for each lattice site, there are in total 36 possible states, conveniently designated as (a, b) ($a, b = 1,..., 6$). An exclusion principle is again applied, so that at the most one particle at each lattice site can have the quantum (a, b). If we use $N_{ab}(\mathbf{x}, t)$ to represent the particle state occupation (a, b) at $\mathbf{x}$ and at time t, then $N_{ab} = 1$ or 0 for the state (a, b), depending on whether the state is occupied by a particle or not, respectively. The basic idea for the collision process is the same as in the original FHP model. The particle configuration, after arrival at each cell, will be redistributed in a way that respects conservation of total mass, momentum, and magnetic intensity, quantities that will be defined later. The detailed collisions can be simple or complex, and can be either simultaneous or sequential, as we will discuss in the next section.

An important property of this model compared with other lattice gas models[1] is that the present model introduces a new type of streaming process called the "bidirectional random walk." During this streaming process, at each time step, a particle in state (a, b) can hop from one site to one of its six nearest neighboring sites either in the direction $\mathbf{e}_a$ with probability $1 - |P_{ab}|$, or in the direction $\text{sign}(P_{ab})\,\mathbf{e}_b$ with probability $|P_{ab}|$. The parameter P_{ab} ($|P_{ab}| \leqslant 1$) is a function of (a, b) only and the determination of P_{ab}, which is crucial in obtaining MHD behavior from the model, will be discussed later. The significance of this nondeterministic streaming is that the direction of motion of any particle is not fixed solely by the "momentum" direction as in the pure fluid case, but also is influenced by the magnetic field. The ratio of the particle streaming in a to b direction represents the effect of the macroscopic velocity and the magnetic field on a single particle, including the effects of the Lorentz force, which is crucial in distinguishing MHD from the hydrodynamics of nonconducting fluids. The bidirectional random walk process introduces stochastic effects in the streaming dynamics of the model. In contrast, in the original FHP lattice gas model stochastic effects enter only through the collision step, for example, through a random choice of clockwise or anticlockwise rotations for two-body head-on collisions. Note that this two-direction streaming scheme does not change the momentum or magnetic field locally.

From the collision and streaming sequence, we can write the general form of the microscopic kinetic equation that determines the evolution of N_{ab}:

$$N_{ab}(\mathbf{x}, t+1) - (1 - |P_{ab}|)\, N_{ab}(\mathbf{x} - \mathbf{e}_a, t) - |P_{ab}|\, N_{ab}(\mathbf{x} - \text{sign}(P_{ab})\,\mathbf{e}_b, t) = \Omega_{ab} \tag{3}$$

The collision operation is denoted by Ω_{ab}, and is interpreted as the change in the population of the state (a, b) as a consequence of all collisions at a specified site and time level. The collision operator includes creation and annihilation effects and is chosen to conserve the total mass, momentum, and magnetic field at each site at each time step. From the exclusion property of the particle occupation for (a, b), Ω_{ab} usually has the form

$$\Omega_{ab} = \sum_{s,s'} (N'_{ab} - N_{ab})\, \zeta(N_{ab} \to N'_{ab})\, \Pi_{a,b} N_{ab}^{N_{ab}} (1 - N_{ab})^{(1 - N_{ab})} \tag{4}$$

Here, $\zeta(s \to s')$ denotes the transition probability from the state N_{ab} before a collision to a state N'_{ab} after a collision. Let us define $f_{ab} = \langle N_{ab} \rangle$ to be the ensemble average of N_{ab}, and let us assume that the quantities that emerge through this averaging process vary on a characteristic macroscopic time scale T and space scale L that are much larger than the microscopic collision time and lattice unit length, respectively. By performing a Taylor expansion, one arrives at the kinetic equation in the continuum form,

$$\partial_t f_{ab}(\mathbf{x}, t) + \{(1 - |P_{ab}|)\, \mathbf{e}_a + P_{ab} \mathbf{e}_b\} \cdot \nabla f_{ab}(\mathbf{x}, t) = \Omega_{ab} \tag{5}$$

where Ω_{ab} is the continuous collision operator obtained from (4) by using f_{ab} instead of N_{ab} and s_{ab} instead of N_{ab} in the exponentials. Here we have defined s_{ab} to be 1 if the state (a, b) is occupied, or 0 otherwise. To obtain this simple expression, we assume also that there are no correlations among different states at the same site and time, i.e., we introduce the Boltzmann approximation.

The macroscopic number density n, momentum $n\mathbf{v}$, and magnetic field $\mathbf{B}$ are defined by

$$\begin{aligned} n &= \sum_{a,b} f_{ab} \\ n\mathbf{v} &= \sum_{a,b} \{(1 - |P_{ab}|)\, \mathbf{e}_a + P_{ab} \mathbf{e}_b\} f_{ab} \\ n\mathbf{B} &= \sum_{a,b} \{Q_{ab} \mathbf{e}_b + R_{ab} \mathbf{e}_a\} f_{ab} \end{aligned} \tag{6}$$

Note that the definitions of velocity and magnetic field are not of the same type as in the familiar FHP model in which the macroscopic velocity field is directly defined as the simple average of the associated microscopic quantity, i.e., $n\mathbf{v} = \sum_{a,b} \mathbf{e}_a f_{ab}$. In the present case the microscopic velocity $\tilde{v}_{ab}$ and magnetic field $\tilde{B}_{ab}$ are defined

$$\begin{aligned} \tilde{v}_{ab} &= \{(1 - |P_{ab}|)\, \mathbf{e}_a + P_{ab} \mathbf{e}_b\} \\ \tilde{B}_{ab} &= \{Q_{ab} \mathbf{e}_b + R_{ab} \mathbf{e}_a\} \end{aligned}$$

Therefore, both directions $\mathbf{e}_a$ and $\mathbf{e}_b$ make contributions to the velocity and the magnetic field.

The parameter matrices P_{ab}, Q_{ab}, and R_{ab} in (6) are chosen to be constants for a given system and to be determined in such a way that if one inserts the quantities in (6) into Eq. (5), the macroscopic moment equations that are obtained will reduce to the MHD equations in (1). Because the MHD system is invariant under proper or improper rotations, it can be shown[14] that the parameter matrices depend only upon $|a-b|$. Furthermore, since the velocity field is a vector field and $\mathbf{B}$ is a pseudovector, the time evolution of the MHD velocity field is unchanged if the magnetic field is reversed everywhere. We make use of this property at the microscopic level and require that $P_{ab} = -P_{ab+3}$, $Q_{ab} = Q_{ab+3}$, and $R_{ab} = -R_{ab+3}$. Hence, there are only six independent parameters in this model. These are chosen to be p_{aa}, p_{aa+1}, q_{aa}, q_{aa+1}, r_{aa}, and r_{aa+1}.

Forming moments of the particle distribution by multiplication of Eq. (5) by 1, $\tilde{v}_{ab}$, and $\tilde{B}_{ab}$ and summing over a and b, one obtains the macroscopic equations for mass, momentum, and magnetic field, which take the form

$$\begin{aligned} &\frac{\partial n}{\partial t} + \nabla \cdot n\mathbf{v} = 0 \\ &\frac{\partial (n\mathbf{v})}{\partial t} + \nabla \cdot \mathbf{\Pi} = 0 \\ &\frac{\partial (n\mathbf{B})}{\partial t} + \nabla \cdot \mathbf{\Lambda} = 0 \end{aligned} \tag{7}$$

where $\mathbf{\Pi}$ and $\mathbf{\Lambda}$ are the momentum flux tensor and the magnetic field flux tensor, respectively. In particular,

$$\mathbf{\Pi} = \sum_{ab} \tilde{v}_{ab} \tilde{v}_{ab} f_{ab}$$

$$\mathbf{\Lambda} = \sum_{ab} \tilde{B}_{ab} \tilde{v}_{ab} f_{ab}$$

3. BOLTZMANN APPROXIMATION AND TRANSPORT COEFFICIENTS

To reduce further the form of Eqs. (7) and thereby obtain the macroscopic equation for MHD, we assume that the microscopic collision processes drive the system rapidly toward a local thermodynamic equilibrium. From the conservation laws of the collision operation, one can prove by

using the H-theorem[3] that the equilibrium should have the Fermi–Dirac form

$$f_{ab}^{(0)} = \frac{1}{1 + \exp(\alpha + \beta \mathbf{e}_a \cdot \mathbf{u} + \eta \mathbf{e}_b \cdot \mathbf{B})} \tag{8}$$

The Lagrange multipliers α, β, and η are functions of η, $\mathbf{v}$ and $\mathbf{B}$ and are determined from the conservation of mass, momentum, and magnetic field by microscopic collisions. Following the Chapman–Enskog expansion scheme, this equilibrium is assumed to be the zeroth-order solution of the collision operator, that is, $\Omega_{ab}^0(f^{(0)}) = 0$.

Under the condition of small velocity $|\mathbf{v}| \ll 1$ and small magnetic field $|\mathbf{B}| \ll 1$, the equilibrium distribution can be expanded and written approximately as

$$\begin{aligned} f_{ab}^{(0)} = {} & \frac{n}{36} + \frac{n}{18}\left(\frac{\mathbf{v}\cdot\hat{e}_a}{\lambda_1} + \frac{\mathbf{B}\cdot\hat{e}_b}{\lambda_2}\right) \\ & + \frac{2n}{18} g(n)\left(\frac{\mathbf{Q}_a : \mathbf{vv}}{\lambda_1^2} + \frac{\mathbf{Q}_b : \mathbf{BB}}{\lambda_2^2}\right) + O(\mathbf{v}^3, \mathbf{v}^2\mathbf{B}, \mathbf{v}\mathbf{B}^2, \mathbf{B}^3) \end{aligned} \tag{9}$$

where

$$\begin{aligned} Q_{aij} &= e_{ai}e_{aj} - \frac{1}{2}\delta_{ij} \\ g(n) &= \frac{18 - n}{36 - n} \end{aligned} \tag{10}$$

and λ_1, λ_2 depend on the matrices P_{ab}, Q_{ab}, and R_{ab}.[14] Substituting (8) and (6) into (5), one can show that n, $\mathbf{v}$, and $\mathbf{B}$ approximately obey the following nondissipative equations:

$$\begin{aligned} \partial_t n + \nabla\cdot(n\mathbf{v}) &= 0 \\ \partial_t(n\mathbf{v}) + \nabla\left[C_1\frac{n}{6} - \frac{1}{2}ng(n)(C_2\mathbf{v}^2 - C_3\mathbf{B}^2)\right] & \\ = -\nabla\cdot ng(n)[C_2\mathbf{vv} - C_3\mathbf{BB}] & \\ \partial_t(n\mathbf{B}) + (D_1 - D_3)\nabla\cdot[ng(n)\,\mathbf{Bv}] + (D_2 + D_3)\nabla\cdot[ng(n)\,\mathbf{vB}] & \\ = D_3\nabla[ng(n)\mathbf{v}\cdot\mathbf{B}] & \end{aligned} \tag{11}$$

The coefficients C_1, C_2, C_3, D_1, D_2, and D_3 depend upon the matrices P_{ab}, Q_{ab}, and R_{ab}; detailed expressions of this dependence have been obtained in ref. 14.

In order to arrive at the complete MHD equations (with diffusive terms), we have to consider the next order approximation in (9). To do that and to obtain the transport coefficients, we have to take into consideration the detailed structure of the collision operator in (4). In the original paper,[14] only simple two-body head-on collisions and three-body symmetric collisions were considered, where these collisions do not allow any nonparticipating "spectators." This definition of the collisions give rise to relatively large transport coefficients, including the kinematic viscosity ν and the magnetic resistivity μ. Physically this structure of the collisions is associated with a low-particle-density limit. In real lattice gas simulations, one generally does not use very low densities to simulate realistic flows, because it leads to long mean free paths and long relaxation times. It is known[15] that the computational work in a two-dimensional lattice gas system is proportional to $Re^{9/4}$ from consideration of the signal-to-noise ratio, where Re is the Reynolds number, inversely proportional to the viscosity. Therefore, in order to reduce computational work, it is desirable for lattice gas models to have low transport coefficients, allowing a simulation of a system with the same Reynolds number but with fewer lattice cells. Moreover, the viscosity is a function of the collision frequency, and usually a high collision frequency will have a low viscosity. In the present model, the phase space for the collisions includes 36 possible states and it would be ideal to allow the collision operator to include all possible collisions (the highest collision frequency) to minimize the transport coefficients. A list of all such possible collisions would require $2^{36} \approx 7 \times 10^{10}$ entries. For a real programming situation, using a table lookup scheme,[9] this table would need about 10 gigabytes of fast memory, which is not possible on most current computers. An alternative would be to use the logical operations to compute the entire Boolean collision integral,[9] but for the present case it would be very tedious and quite complicated to write down the complete logic for all possible collisions. In addition, a program that computed such a large number of collisions directly would be extremely inefficient.

In the present implementation of the MHD lattice gas model, in order to strike a reasonable compromise between the Reynolds number requirement and the efficiency of the computations, we introduce the following two-step "sequential" collision algorithm:

(1) Three-body collisions: at each lattice cell and for each collision time step, we first implement the three-body collision operation. For this step, we look at all possible three-particle symmetric configurations in each cell (up to 12) that allow for particle scattering. At the same time, we also classify all three-hole symmetric configurations which would be able to

accept particles after a possible scattering event. Then we randomly pick one pair of these particle and hole configurations and interchange their populations (i.e., the particles and holes are interchanged). After this step, we will carry out the same procedure sequentially for the other sets of states, in a predetermined order. This process will continue until we cannot find any more pairs of three-particle and three-hole symmetric configurations. Actually, the number of such three-body scattering events in a particular cell number will be the minimum of the number of three-particle configurations and the number of three-hole configurations, since the operation is restricted by the exclusion rule of the model. Note that for each collision, we do not care whether or not the other states are occupied. Thus, each actual collision could be taking place in a cell having many particles. In fact there can be up to 30 "spectator" particles during a specific interchange of three particles and three holes. Thus, we can see that the present collision scheme allows many more collision possibilities than the original lattice gas model, for example, the FHP-I model and the model presented in ref. 14, where only purely three-body collision are considered.

(2) Two-body head-on collisions: After the three-body collision step, we will have a new particle and hole configuration in each lattice. The following two-body head-on collision procedure begins from this new configuration. The basic idea for the two-body collisions is the same as for the three-body case. All the states are logically scanned for the occurrence of occupied head-on particle states and unoccupied head-on hole states. Using a randomly selected sequence, the pairs of matched holes are interchanged with the pairs of matched particles until the supply of either set of pairs is exhausted. The logic for this operation is straightforward to code and efficient to execute using Boolean masks with no branching.

From the computational point of view, the above-described sequential collision algorithm does not need a large amount of memory to deal with all possible configurations. Instead, it needs at most only 6 bits (per cell in a parallel implementation) at each time step for three-body collisions, which have the simple form

$$f_{a,b} f_{a+2,b+2} f_{a+4,b+4} (1 - f_{a',b'})(1 - f_{a'+2,b'+2})(1 - f_{a'+4,b'+4})$$

and 4 bits for two-body collisions, which have the form $f_{a,b} f_{a+3,b+3} (1 - f_{a',b'})(1 - f_{a'+3,b'+3})$, where we require that $(a, b) \neq (a', b')$.

For this two-step sequential collision process, the general collision operator has the form

$$\Omega_{ab} = \Omega^3_{ab}(f) + \Omega^2_{ab}(f')$$

In $\Omega^3_{ab}(f)$, we use the quantity f at the time step t, while in $\Omega^2_{ab}(f')$ we use the new f' that can be written as $f'_{ab} = f_{ab}(\mathbf{x}, t) + \Omega^3_{ab}(f(\mathbf{x}, t))$. The detailed collision operators can be written as

$$\Omega^3_{ab}(f) = \prod_{c,d}(1 - f_{cd}) \sum_{efg} \left[S^{3A}_{efg} \tilde{f}_{ea+1} \tilde{f}_{fa+3} \tilde{f}_{ga+5} + S^{3B}_{efg} \tilde{f}_{ea} \tilde{f}_{fa+2} \tilde{f}_{ga+4} - \sum_{ef} S^{3}_{ef} \tilde{f}_{ba} \tilde{f}_{ea+2} \tilde{f}_{fa+4} \right]$$

and

$$\Omega^2_{ab}(f) = \prod_{c,d}(1 - f_{cd}) \sum_{ef} \left[S^{2L}_{ef} \tilde{f}_{ea+1} \tilde{f}_{fa+4} + S^{2R}_{ef} \tilde{f}_{ea+2} \tilde{f}_{fa+5} + S^{2B}_{ef} \tilde{f}_{ea} \tilde{f}_{fa+3} - \sum_{e} S^{2}_{e} \tilde{f}_{ba} \tilde{f}_{ea+3} \right]$$

which correspond to the three- and two-body particle collisions. In the above equations, $\tilde{f}_{ab} = f_{ab}/(1 - f_{ab})$. The coefficient S^{3A} is the probability for having input populations at a specific site without a particle in the particular state (a, b). The coefficient S^{3B} is the probability for an output population with the state (a, b) occupied by a particle, for the case in which the collisions have changed only the b vectors. The coefficient S^3 is the probability for all collisions in which the population initially included a particle occupying the state (a, b), but in which this state is unoccupied in the output population, and, in addition, the scattering out of (a, b) is affected by changing both the a and b indices of the originally resident particle. The coefficients S^{2L} and S^{2R} are the probabilities for particles coming into the state (a, b) after a left or right rotation, respectively, of their a and b vectors. This notation has been used previously by Wolfram.[2] The coefficient S^{2B} is the probability for two-particle head-on particle collisions in which the a vectors do not change after the collision, but the b vectors do change. Finally, the coefficient S^2 denotes probability of two-body head-on collisions which cause the state (a, b) to become unoccupied.

From the definition of $\tilde{B}_{ab}$, the conservation of magnetic field requires that the three-body collisions happen only when they have symmetric b vectors, a condition that can be written as

$$\begin{aligned} S^{3A}_{efg}(b) &= \delta(e - f + 2)\, \delta(e - g + 4)\, S^{3A}_{e}(b) \\ S^{3B}_{efg}(b) &= \delta(e - f + 2)\, \delta(e - g + 4)\, S^{3B}_{e}(b) \\ S^{3}_{ef}(b) &= \delta(b - e + 2)\, \delta(b - f + 4)\, S^{3}(b) \end{aligned} \tag{12}$$

Similarly, the two-body collision probability has the form

$$\begin{aligned} S_{ef}^{2L}(b) &= \delta(e-f+3)\, S_e^{2L}(b) \\ S_{ef}^{2R}(b) &= \delta(e-f+3)\, S_e^{2R}(b) \\ S_{ef}^{2}(b) &= \delta(e-f+3)\, S_e^{2}(b) \end{aligned} \tag{13}$$

Assuming that f_{ab} departs only slightly from the state of equilibrium, we have

$$\begin{aligned} f_{ab} &= f_{ab}^{(0)} + f_{ab}^{(1)} \\ |f_{ab}^{(1)}| &\ll f_{ab}^{(0)} \end{aligned}$$

Then Eq. (5) can be written to first order as

$$\partial_t f_{ab}^{(0)}(\mathbf{x}, t) + \{(1-|P_{ab}|)\,\hat{e}_a + P_{ab}\hat{e}_b\} \cdot \nabla f_{ab}^{(0)}(\mathbf{x}, t) = \Omega_{ab}^{(1)} \tag{14}$$

where $\Omega_{ab}^{(1)} = \sum_{\sigma,\lambda} C_{ab,\sigma,\lambda}^{(0)} f_{ab}^{(1)}$. The $C_{ab,\sigma,\lambda}^{(0)}$ are the linear expansion coefficients from the collision operator in (4). Considering the effects of sequential collision, and after some simple algebra, one obtains that

$$C_{ab,\sigma,\lambda}^{(0)} = (\mathbb{1} + C_{ab,\sigma,\lambda}^{(0)(2)})(\mathbb{1} + C_{ab,\sigma,\lambda}^{(0)(3)}) - \mathbb{1}$$

Here, $C^{(0)(3)}$ denotes the linear expansion matrix derived from the symmetric three-body collision operator Ω_{ab}^{3}, and $C^{(0)(2)}$ denotes the linear expansion matrix derived from the head-on two-body collision operator $\Omega_{ab}^{(2)}$, while $\mathbb{1}$ is the unit matrix. In both $C^{(0)(3)}$ and $C^{(0)(2)}$, only $f^{(0)}(\mathbf{x}, t)$ is used. Note that in general $C^{(2)}C^{(3)} \neq C^{(3)}C^{(2)}$, which represents the fact that the two steps of the sequential collision process do not commute. The three-body step is implemented first to minimize spurious conservation effects.

Following refs. 14 and 9, and after some very tedious algebra, we obtain the kinematic viscosity ν,

$$\begin{aligned} \nu = \frac{1}{27\lambda_1 \xi_1} &(|p_{aa+1}| - |p_{aa}| + p_{aa} - 2p_{aa+1})\{(1-|p_{aa}|)^2 - (1-|p_{aa+1}|)^2 \\ &+ 2(1-|p_{aa}|)\, p_{aa} - 4(1-|p_{aa+1}|)\, p_{aa+1} + |p_{aa}|^2 - |p_{aa+1}|^2\} + \nu_l \end{aligned} \tag{15}$$

the bulk viscosity ν_d,

$$\begin{aligned} \nu_d = \frac{1}{9\lambda_1 \xi_3} &\left(|p_{aa+1}| - |p_{aa}| + p_{aa} - \frac{1}{2} p_{aa+1}\right)[(1-|p_{aa}|)^2 - (1-|p_{aa+1}|)^2 \\ &+ 2(1-|p_{aa}|)\, p_{aa} - (1-|p_{aa}|)\, p_{aa+1} + |p_{aa}|^2 - |p_{aa+1}|^2] \end{aligned} \tag{16}$$

the magnetic resistivity μ,

$$\mu = \frac{1}{54\lambda_2}\left\{\frac{2}{\xi_1}(3 - |p_{aa}| - 2|p_{aa+1}| + p_{aa} + p_{aa+1})[q_{aa}(1 - |p_{aa}|) + 2q_{aa+1}(1 - |p_{aa+1}|) + 2r_{aa+1}p_{aa+1} + r_{aa+1}(1 - |p_{aa+1}|) + q_{aa}p_{aa} + q_{aa+1}p_{aa+1}] + \frac{27}{2\xi_3}(1 - |p_{aa+1}|)[q_{aa+1}(1 - |p_{aa+1}|) - r_{aa+1}p_{aa+1}]\right\} + \mu_l \quad (17)$$

and the bulk magnetic resistivity μ_d,

$$\mu_d = \frac{1}{18\lambda_2}\left\{\frac{1}{\xi_2}(|p_{aa+1}| - |p_{aa}| + p_{aa} - 2p_{aa+1})[q_{aa}(1 - |p_{aa}|) - q_{aa+1}(1 - |p_{aa+1}|) - r_{aa+1}p_{aa+1} - 2r_{aa+1}(1 - |p_{aa+1}|) + q_{aa}p_{aa} - 2q_{aa+1}p_{aa+1}] + \frac{2}{\xi_3}\left[\frac{3}{2} - |p_{aa}| - \frac{1}{2}|p_{aa+1}| + p_{aa} + p_{aa+1}\right]\left[q_{aa}(1 - |p_{aa}|) + \frac{1}{2}q_{aa+1}(1 - |p_{aa+1}|) + \frac{1}{2}r_{aa+1}p_{aa+1} + r_{aa+1}(1 - |p_{aa+1}|) + q_{aa}p_{aa} + q_{aa+1}p_{aa+1}\right] - \frac{9}{2\xi_3}(1 - |p_{aa+1}|)[q_{aa+1}(1 - |p_{aa+1}|) - r_{aa+1}p_{aa+1}]\right\} \quad (18)$$

In the above equations,

$$\lambda_1 = 1 - \frac{1}{3}(|p_{aa}| + 2|p_{aa+1}| - p_{aa} - p_{aa+1})$$

$$\lambda_2 = \frac{1}{3}(q_{aa} + 2q_{aa+1} + r_{aa+1} + r_{aa})$$

$$\xi_1 = (1 - 3k_1)(1 - 24k_2) - 1$$

$$\xi_2 = (1 - 6k_1)(1 - 24k_2) - 1$$

$$\xi_3 = 72k_1k_2$$

$$k_1 = S^2d(1 - d)^2$$

$$k_2 = 6S^{3B}d^2(1 - d)^3$$

and ν_l and μ_l are the lattice viscosity and the lattice magnetic, resistivity, respectively, from the particle streaming in the discrete space:

$$\nu_l = \frac{1}{24\lambda_1}\left[(1-|p_{aa}|)^2 + 2(1-|p_{aa+1}|)^2 + p_{aa}|p_{aa}| + p_{aa+1}|p_{aa+1}| + 6|p_{aa+1}|(1-|p_{aa+1}|)\right]$$

$$\mu_l = \frac{1}{24\lambda_2}\left[q_{aa} + q_{aa+1}(5-3|p_{aa+1}|) + r_{aa+1}\right]$$

In deriving the equations above, we have assumed that $S^{3A} = S^{3B} = S^3$ and $S^{2L} = S^{2R} = S^2$ from consideration of rotational symmetry of the collisions.

In Figs. 1 and 2, we present the analytical results for the kinematic viscosity and the magnetic resistivity (solid lines and the right vertical axis) as a function of density per state d for a typical case: $p_{aa} = -0.2000$, $r_{aa} = 0$, $p_{aa+1} = 0.1009$, $q_{aa} = 1.7800$, $q_{aa+1} = 0.1349$, $r_{aa+1} = -1.2030$ ($C_1 = 2.179$ and $C_2 = 1.032$). The parameters $S^2 = 1/6$ and $S^{3B} = 1/12$ are used, which should be close to the real situations in the coding discussed above. However, since a real numerical implementation would use the maximum possible number of sequential collisions for each lattice cell, it can be expected that the analytically obtained viscosity should be a little bigger than the simulation results. From these two plots, one can see that the increase of density will lead to a decrease of transport coefficients. This tendency agrees with other lattice gas models.[6] The viscosity and resistivity for the original model have also been given in Figs. 1 and 2 for comparison (using the dashed lines and the left vertical axis). As pointed out before, the present model with higher frequency of collisions gives much smaller transport coefficients. We see that the current model gives about two orders of magnitude smaller viscosity and resistivity than the original model.

In order to compare the analytical results for the transport coefficients with simulation, we perform numerical measurements of the transport coefficients in the present model using the following two methods:

(i) Forced channel flow with no magnetic field.

The idea of using a forced channel flow to measure the kinematic viscosity in lattice gases has been described previously.[16] For pure one-dimensional channel flow, the momentum equation will have a very simple form:

$$\nu \frac{d^2 u_x(y)}{dy^2} = f = \text{const}$$

Here u_x is the velocity along the channel direction, and is dependent only on the y direction. f is the forcing rate for unit area at each time step. For the nonslip boundary condition, u_x has a parabolic form. The relation between the forcing and the viscosity of the system has a simple form:

$$v = \frac{fW^2}{8j_{\max}} \tag{19}$$

where W is the channel width and $j_{\max}$ is the maximum velocity (in the center of the channel). In the simulation, the forcing is implemented by flipping particle directions[16] randomly in space for each time step. In order that the particle flipping only changes the momentum field and does not induce any change in the magnetic field, one must carefully choose the state (a, b) that is allowed to be forced. Suppose that the flow direction is along x. In order to have a stable flow, one could change the particle direction of a particle in state (a, b) by flipping its a coordinate to increase the momentum in the x direction. This could be accomplished by changing particles moving in directions 3, 4, and 5 to directions 2, 1, and 6, respectively, regardless of b, as done in the FHP-type lattice gas models.[16] However, from (6), one can find that the only particle flipping that ensures that there is no magnetic field induced is going from a configuration with a particle with direction a change to another with a particle in the direction $a+3$. Moreover, if we are only interested in a forcing in the channel direction, from the microscopic velocity definition, the a direction must be in the direction parallel to the forcing direction, i.e., 4 and 1. Otherwise, there would be an additional forcing added in the vertical direction.

Using a forced channel flow and Eq. (19), we have measured viscosities for lattice gas systems with the complete collision operator in the sequential version. In Fig. 1, we present the simulation results (square symbol) for viscosity as a function of density per state d compared with analytical results (solid line). The simulation has been done for a system with the same parameters used in the analytical curve. The typical lattice gas system size is 256×128. In order to have a zero velocity in the boundary, we allow the upper half-space (with 64 lattice layers) to be forced in the positive x direction and the lower half-space to be forced in the negative x direction. Periodic conditions have been used for both x and y directions. The initial configuration of the system has a zero velocity. We run about 20,000 time steps to allow the system to approach a local equilibrium state, then time average over the next 20,000 time steps and space average in the x direction to obtain a velocity distribution. As we expected, the viscosities in the simulation are smaller than the analytical results due to the higher collision frequency in the real simulation.

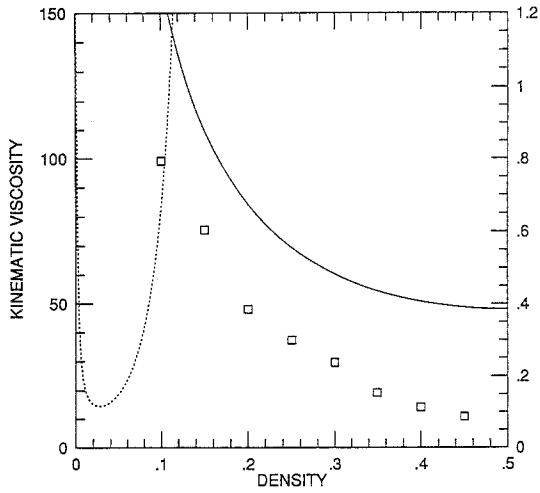

Fig. 1. Viscosity as function of density for the MHD CA model. Solid line, associated with the vertical axis on the right side, is the analytical result for the approximate treatment of the sequential collision method described in the text. The dotted line (left vertical scale) is the analytical result from the original formulation of the model, using only two- and three-body collisions with no spectators. (□) The values of the viscosity obtained from numerical simulations of a forced channel flow, also described in the text. The sequential collisions give viscosities nearly two orders of magnitude smaller than the earlier model with only two- and three-body collisions.

(ii) Free-decay system.

An alternative method to measure the transport coefficients is to use a simple decaying flow system, by which we measure the resistivity of the present MHD lattice gas model.[17] For an unforced system with periodic boundaries (or infinite system), the one-dimensional MHD problem is reduced to a pure diffusion equation

$$\frac{\partial B_x}{\partial t} = \mu \nabla^2 B_x$$

If B_x only depends on the y coordinate and the initial condition is a sinusoidal field $B_x(0) = B_0 \sin(ky)$, then the solution can be written as

$$B_x(y, t) = B_x(0) \exp(-\mu k^2 t) \tag{20}$$

By measuring the decay rate of this sinusoidal B_x field, one can obtain the resistivity. In Fig. 2, we present the numerical measurement results of μ (represented by the square symbol) as a function of particle number per state. A system of 8192×256 is used. $B_x(0) = 0.1$ and $k = 2\pi/256$. The

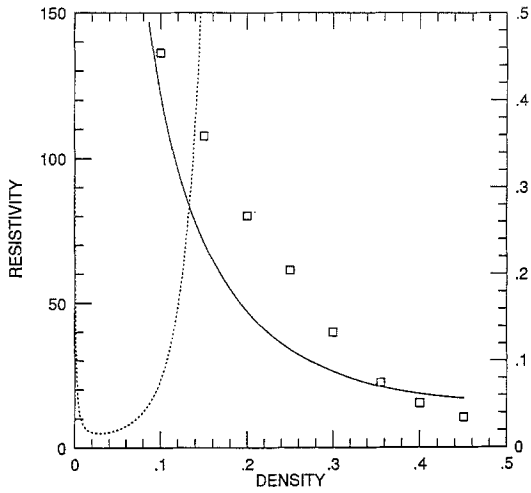

Fig. 2. Resistivity as a function of density for the MHD CA model. Solid line (scale on right vertical axis) is the analytical result for the approximate treatment of the sequential collision method described in the text. The dotted line (left vertical axis) is the analytical result from the original formulation of the model, using only two- and three-body collisions with no spectators. (□) The values of the resistivity obtained from numerical simulations of a freely decaying magnetic field, also described in the text. The present model with sequential collisions gives resistivities much smaller than those in the earlier formulation of the model.

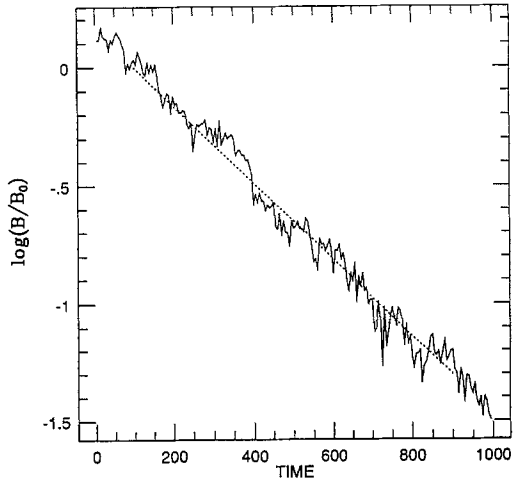

Fig. 3. Decay of the magnetic field intensity, shown on a log scale, versus time, for a typical freely decaying magnetic field simulation with the MHD CA model with sequential collisions. The behavior is close to exponential in time, and serves to determine the value of the resistivity.

resistivity is obtained by averaging the decay rate μ at each line. The exponential decay of B_x can be seen from simulations. A typical decay plot for B_x/B_0 is given in Fig. 3. One can see from Fig. 2 that the simulations again have a good agreement with the analytical results.

4. SOUND WAVES AND ALFVÉN WAVES

Let us consider a small disturbance of a uniform fluid system with a constant magnetic field:

$$\begin{aligned} n &= n_0 + \delta n \\ B_i &= B_{0i} + \delta B_i \\ v_i &= \delta v_i \end{aligned} \tag{21}$$

with $n_0 = \text{const}$, $B_{0i} = \text{const}$, $|\delta n| \ll n_0$, $|\delta B_i| \ll |B_{0i}|$, and $|\delta v_i| \sim \delta n$. Inserting (21) into the first equation in (7) and (11) for a nondissipative case, to the first order in δn, $\delta \mathbf{v}$, and $\delta \mathbf{B}$, we have

$$\frac{\partial(\delta n)}{\partial t} + n_0 \frac{\partial(\delta v_i)}{\partial x_i} = 0 \tag{22}$$

$$\begin{aligned} n_0 \frac{\partial(\delta v_i)}{\partial t} = &-\frac{C_1}{6}\frac{\partial}{\partial x_i}(\delta n) \\ &+ C_2 \frac{\partial}{\partial x_j}[n_0 g(n_0)(B_{0j}\delta B_i + \delta B_j B_{0i}) + \tilde{g}\delta n B_{0j} B_{0i}] \\ &- \frac{C_2}{2}\frac{\partial}{\partial x_i}[n_0 g(n_0)(B_{0j}\delta B_j + \delta B_j B_{0j}) + \tilde{g}\delta n B_{0j}^2] \end{aligned}$$

$$n_0 \frac{\partial(\delta B_i)}{\partial t} + B_{0i}\frac{\partial}{\partial t}(\delta n) = C_2 n_0 g(n_0)\frac{\partial}{\partial x_j}[B_{0j}\delta v_i - \delta v_j B_{0i}] \tag{23}$$

where $\tilde{g} = g(n_0) + n_0 g'(n_0)$ and $g'(n_0) = -18/(36 - n_0)^2$.

We make use of the Laplace–Fourier transformation

$$\tilde{W}(\mathbf{k}, s) = \int_0^\infty dt\, e^{-st} \int_{-\infty}^{\infty} e^{i\mathbf{k}\cdot\mathbf{r}} W(\mathbf{r}, t)\, d\mathbf{r} \tag{24}$$

where W could be any one of δn, $\delta \mathbf{v}$, or $\delta \mathbf{B}$. Then from (23) and (24), we have the dispersion relation

$$\begin{vmatrix} s & i\mathbf{k} & 0 \\ i\hat{M}_1 \cdot \mathbf{k} & s\mathbb{1} & C_2 g(n_0)\, i[\mathbf{k}\mathbf{B}_0 - \mathbf{B}_0\mathbf{k}] \\ s\mathbf{B}_0 & -iC_2 g(n_0)[\mathbf{B}_0 \cdot \mathbf{k}\mathbb{1} - \mathbf{B}_0\mathbf{k}] & s\mathbb{1} \end{vmatrix} = 0 \tag{25}$$

where $\hat{M}_1 = [(C_1/6 + \frac{1}{2}C_2 B_0^2 \tilde{g})\mathbb{1} - C_2 \tilde{g}\mathbf{B}_0\mathbf{B}_0]$.

For the pure fluid case, $B_i = 0$, Eqs. (25) give the simple relation $s/k = (C_1/6)^{1/2}$ and (23) will give a sound wave propagation equation for the density fluctuation and velocity fluctuation, such as

$$\frac{\partial^2 \delta n}{\partial t^2} = c_s^2 \nabla^2 \delta n$$

with the sound speed $c_s = (C_1/6)^{1/2}$. The sound speed is a property of the system, and for the present lattice gas model, this sound speed is a function only of C_1. In addition, we know[14] that C_1 depends only upon p_{aa} and p_{aa+1}. Thus, the sound speed here is affected by the random walk of the particles only.

After eliminating the velocity terms in (23), we obtain an equation for δB_i:

$$\begin{aligned}
\frac{\partial^2}{\partial t^2}\delta B_i = {} & B_{0i}[1 - C_2 g(n_0)] \frac{1}{n_0}\left\{ -\frac{C_1}{6}\frac{\partial^2 \delta n}{\partial x_j^2} \right. \\
& + C_2 n_0 g(n_0) \frac{\partial^2}{\partial x_j \partial x_k}(B_{0k}\delta B_j + \delta B_k B_{0j}) \\
& \left. + \tilde{g} B_{0k} B_{0j} \frac{\partial^2 \delta n}{\partial x_k \partial x_j} - C_2 n_0 g(n_0) \frac{\partial^2}{\partial x_j^2} B_{0k}\delta B_k - \frac{C_2}{2}\tilde{g} B_{0k}^2 \frac{\partial^2 \delta n}{\partial x_j^2} \right\} \\
& + C_2 g(n_0) B_{0k} \frac{1}{n_0}\left\{ -\frac{C_1}{6}\frac{\partial^2 \delta n}{\partial x_i \partial x_k} \right. \\
& + C_2 \frac{\partial^2}{\partial x_j \partial x_k}[n_0 g(n_0)(B_{0j}\delta B_i + \delta B_j B_{0i}) + \tilde{g}\delta n B_{0j} B_{0i}] \\
& \left. - \frac{C_2}{2}\frac{\partial^2}{\partial x_i \partial x_k}[n_0 g(n_0)(B_{0j}\delta B_j + \delta B_j B_{0j}) + \tilde{g}\delta n B_{0j}^2] \right\} \qquad (26)
\end{aligned}$$

If we choose a special case with $B_{0x} = 0$ and $B_{0y} = B_0$, from (23), we get

$$\begin{aligned}
\frac{\partial^2(\delta B_x)}{\partial t^2} = {} & C_2^2 g^2(n_0) B_0^2 \frac{\partial^2}{\partial y^2}\delta B_x - C_2^2 g^2(n_0) B_0^2 \frac{\partial^2}{\partial x\, \partial y}\delta B_x \\
& - C_2^2 \frac{g(n_0)}{n_0} B_0^3 \frac{\partial^2}{\partial x\, \partial y}\delta B_x - C_2^2 \frac{g(n_0)}{n_0} B_0^3 \frac{\partial^2}{\partial x\, \partial y}\delta n \qquad (27)
\end{aligned}$$

For low Mach number, we assume that $\delta n \ll \delta B_x$; we can drop the last term in the above equation. The second and third terms on the right-hand side of (27) come from the nonphysical terms (proportional to B^2) in the equation of state. Suppose that the flow in the x direction is homogeneous,

and we then average the above equation in the x direction. This produces the wave equation

$$\frac{\partial^2}{\partial t^2}\delta B_x(y,t) - C_B^2 \frac{\partial^2}{\partial y^2}\delta B_x(y,t) = 0 \tag{28}$$

where $C_B = C_2\, g(n_0)\, B_0$ is the Alfvén speed. The solutions are Alfvén waves, in which the x component of the magnetic field propagates parallel or antiparallel to the mean magnetic field direction at the Alfvén speed. The dependence of the Alfvén wave speed on the parameter C_2 is caused by the particle random walk effect of the present model and the $g(n)$ effect represents the non-Galilean effect of the model on the magnetic wave propagation, which usually reduces the Alfvén speed. One can derive a similar equation for the propagation of δB_y along a mean magnetic field in the x direction.

In order to verify the results obtained above, we use the lattice gas simulation to measure the sound and Alfvén wave speeds. The measurements can be done by measuring the power spectrum (Laplace transform of the two-time correlation function[18]) in the long-wave limit for density and magnetic field. The magnetic field power spectrum $\langle \mathbf{B}(\mathbf{k}, s)\, \mathbf{B}^*(\mathbf{k}, 0)\rangle / \langle \mathbf{B}(\mathbf{k}, 0)\, \mathbf{B}^*(\mathbf{k}, 0)\rangle$ and the density power spectrum $\langle n(\mathbf{k}, s)\, n^*(\mathbf{k}, 0)\rangle / \langle n(\mathbf{k}, 0)\, n^*(\mathbf{k}, 0)\rangle$ will have a Lorentzian form: $s/(s^2 + a^2k^2)$. Here a is either the sound speed C_s or the Alfvén speed C_B.

For measuring the sound propagation, we use 8192×256 lattice cells with a zero mean velocity field and zero mean magnetic field. An average in the x direction is used to replace the ensemble average, motivating the choice of a lattice that is much bigger in the x direction than in the y direction. Thus, only the propagation of the velocity fluctuation in the y direction is measured.

A typical power spectrum of the density correlation is shown in Fig. 4 as a function of ω for $p_{aa} = -0.2$, selecting only the contributions due to fluctuations with wavenumber $k = 1$. The figure shows a very sharp resonance, corresponding precisely to the solution of the dispersion relation with the same parameters. In Fig. 5, we present a measurement of the sound speed versus the parameter C_1 (obtained by varying the streaming parameter p_{aa} for the solution in ref. 14). We see that the sound speed of the system changes with the variation of the random walk parameter p_{aa}. It is interesting to see that the sound speed could be much smaller than the sound speed in the FHP lattice gas of $1/\sqrt{2}$. This feature has a potential application for simulating supersonic flows, and one could vary p_{aa} to obtain different values of the Mach number.

For simulating Alfvén waves, again a system of 8192×256 lattice cells is used. Periodic conditions have been used for both the x and y directions.

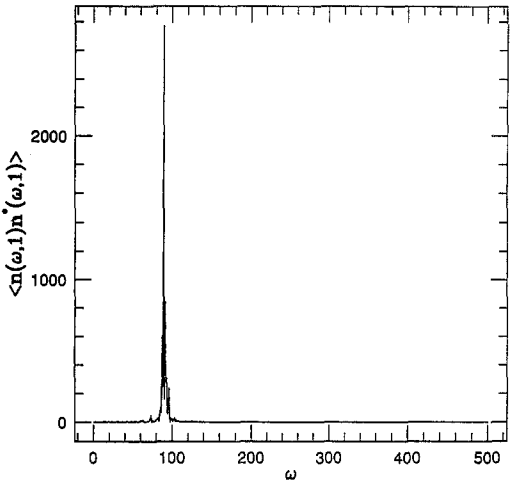

Fig. 4. Power spectrum of the density field, as a function of frequency, for fluctuations with wavenumber $k = 1$, showing a sharp resonance at a frequency corresponding to the solution of the sound wave dispersion relation.

Initially a magnetic field is imposed along the y direction of amplitude B_0, whereas B_x and $\mathbf{v}$ are random and statistically zero. For a small magnetic field B_0, Eq. (9) should be a good approximation for real equilibrium to begin with, which satisfies the physical constraint $0 \leqslant f_{ab} \leqslant 1$. For a bigger B field, actually for the parameters listed in Table I in ref. 14, when

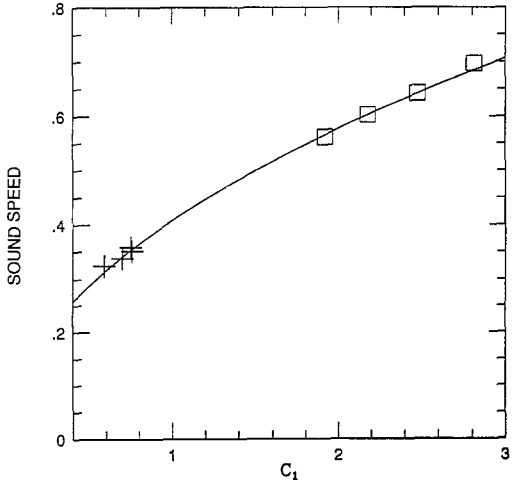

Fig. 5. Numerical measurements of the sound speed in the MHD CA model, obtained by varying the streaming parameter p_{aa}, shown by the symbols (branch I: squares; branch II: crosses), and compared with the analytical result, shown as a solid line.

$B > 0.16$, f_{ab} does not satisfy this restriction. Thus, the expansion (9) should be replaced by the exact equilibrium expression in (8). The distribution function usually cannot be evaluated in closed form for arbitrary specified velocity and magnetic fields. Fortunately for the special case of B_0 in a particular direction between two lattice links, the distribution $f_{ab}^{(0)}$ can be exactly obtained by solving a cubic equation for α and η when $\mathbf{v} = 0$:

$$A^+A^-H_1^3 - H_1^2[A^+A^- + (A^+ + A^-)] - H_1[A^+A^- - 2(A^+ + A^-) + 3] - A^+A^- + 3(A^+ + A^-) - 9 = 0 \tag{29}$$

and

$$H_2 = \frac{1 + (1 + H_1)(2 - A^+)}{H_1[A^+(1 + H_1) - 1]} \tag{30}$$

with $H_1 \geqslant 0$ and $H_2 \geqslant 0$. In the above equations,

$$H_1 = e^{\alpha}$$

$$H_2 = \exp(\eta B_0 \cdot 3^{1/2}/2)$$

and

$$A^{\pm} = \frac{n}{12} \pm \frac{nB_0}{2\sqrt{3}} \frac{1}{q_{aa} + 2q_{aa+1} + r_{aa+1}}$$

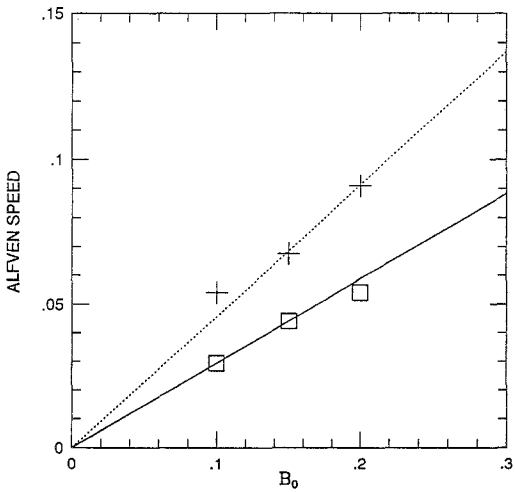

Fig. 6. Dependence of the Alfvén speed in the MHD CA model as the value of the uniform magnetic field is varied. For fractional density 0.1, the dotted line is the analytical result and the crosses are the results obtained by numerical simulation. For fractional density 0.3, the solid line is the analytical result and the squares are the numerical simulation results.

In order for the system to approach equilibrium, it is allowed to run 5000 time steps without computing any macroscopic quantity. During the next 16384 time steps, B_x is obtained for each time step and averaged for each row, so that it has only a y dependence. In Fig. 6, we show the simulation measurement of Alfvén wave speed versus magnetic intensity B_0 compared with analytical results for density 0.1 and 0.3. The solid and dashed lines are the analytical results for density 0.1 and 0.3, respectively, and the $\times$ and $\square$ signs represent the simulation results for density 0.1 and 0.3, respectively. This numerical experiment indicates good agreement between the theoretical Alfvén speed and the Alfvén speed obtained in the simulations.

5. CONCLUSIONS AND DISCUSSIONS

In this paper we have described a lattice gas (cellular automaton) model for magnetohydrodynamic systems, based on the model previously derived by Chen *et al.*[13,14] The model utilizes a 36-bit representation of particle states at each lattice node, incorporating an exclusion principle to maintain a simple logical and Boolean structure. As in the FHP model, the dynamics of particles residing on the lattice consists of streaming and collisions that conserve specified macroscopic quantities. However, in the present model the streaming is nondeterministic and bidirectional, to account for the influences of the Lorentz force on the MHD fluid. Collisions are specified to conserve particle number, momentum, and magnetic field intensity, corresponding to the macroscopic MHD variables. Taking into consideration the symmetries of the MHD model and several constraints, the model reduces to a family of MHD lattice gas models, differing according to a single streaming probability coefficient.

Apart from discussing a number of details of the implementation, the model presented here also extends previous work by describing a sequential collision procedure that allows for transport coefficients that are up to two orders of magnitude smaller than those obtained in the original model. This permits simulations to be done at much higher Reynolds numbers for a given lattice size, opening up the possibility for computation of a greater variety of nonlinear effects, such as turbulence, in an MHD lattice gas context. Similar sequential collision procedures may be also helpful in implementations of other lattice gas models.

Some of the main results presented in the paper pertain to the viscosity and resistivity, which have been computed analytically in an approximate way and compared favorably to simulation results in forced and decaying flows. As predicted by the theory, the numerical results show much smaller transport coefficients (higher Reynolds numbers) than in the

original formulation of the model. In addition, we examined the two most important normal modes of the model, the sound wave and the Alfvén wave, from both analytical and numerical perspectives. Both wave modes are found to behave in a physically reasonable way in the theory, with wave speeds partially controllable by the choice of the bidirectional streaming parameters. In particular, the sound speed can be much smaller than in the FHP model, opening up the possibility of relatively higher Mach number simulations with the present model. Finally, the numerically computed behavior of both the sound wave and the Alfvén wave are found to agree well with the theoretical calculations.

We conclude that the 36-bit MHD lattice gas model with sequential collisions can reproduce at least several of the most basic types of MHD behavior that would be seen in real physical systems and in MHD solutions obtained with more standard methods. Although the present paper has not examined the deficiencies of the model in great detail, we acknowledge that certain shortcomings need to be addressed further. For example, the model has a relatively low signal-to-noise ratio, which at the present time prevents the model from being competitive with standard methods, such as spectral methods, in terms of efficiency and accuracy. Although this problem also plagues other lattice gas models, it is exacerbated in the present model by the additional randomness associated with the nondeterministic bidirectional streaming process. Second, the bidirectional streaming also introduces complications in implementations of boundary conditions. We have investigated a number of ways of enforcing boundary conditions in a statistical way (results not shown here), and found that these methods are unacceptably noisy or unstable. For all of the simulations shown in the present paper, we were able to avoid these complications, but it appears to be quite difficult to enforce the range of MHD boundary conditions that one would like to use for real problems. For example, we have not been able to find an algorithm for effectively enforcing perfectly conducting conditions over an arbitrarily shaped boundary. Finally, we have not addressed further the inherent problem of limiting or eliminating the nonzero divergence of the magnetic field. This difficulty was described in the original formulation of the MHD lattice gas model,[13,14] where it was argued that diffusion effects may prevent large values of this nonphysical quantity in freely-decaying flows. But we are unable to predict the decay speed of this nonzero divergence at the moment. In addition, we have found in the numerical experiments described here that typical values of $\nabla \cdot \mathbf{B}$ remain acceptably small. A modification to the method that would effectively eliminate $\nabla \cdot \mathbf{B}$ in the solutions would appear to be required before the current lattice gas method could be viewed as robust enough for general MHD computations. Recently, we have developed a new lattice

Boltzmann method following the basic model discussed in previous papers[13,14] and this paper. We have found[19] that the lattice Boltzmann method will keep zero divergence of the magnetic field for a very long time if the initial condition is divergenceless. On the positive side, the model admits a number of useful features in parallel computing environments, and it has been shown here to display accurately a number of basic but essential aspects of magnetohydrodynamic flows. Thus we are led, as are others investigating lattice gas models for a variety of systems, to remain optimistic that the lattice gas approach to computation, such as the present MHD model, may represent a new direction for pursuing large-scale fluid and MHD research in the future.

ACKNOWLEDGMENTS

We thank Dr. G. D. Doolen for helpful discussions. This work was supported by the NASA Innovative Research Program under grant NAGW-1648.

REFERENCES

1. U. Frisch, B. Hasslacher, and Y. Pomeau, *Phys. Rev. Lett.* **56**:1505 (1986).
2. S. Wolfram, *J. Stat. Phys.* **45**:19–74 (1986).
3. U. Frisch, D. d'Humières, B. Hasslacher, P. Lallemand, Y. Pomeau, and J.-P. Rivet, *Complex Systems* **1**:649–707 (1987).
4. G. D. Doolen, ed., *Complex Systems* **1**(4):545–851 (1987). [Articles mostly based on presentations given at the Workshop on Large Nonlinear Systems, Santa Fe, New Mexico, October 27–29, 1986.]
5. G. D. Doolen, ed., *Lattice Gas Methods for PDEs* (Addison-Wesley, 1989).
6. D. d'Humières, P. Lallemand, and G. Searby, *Complex Systems* **1**:333–350 (1987).
7. D. H. Rothman and J. M. Keller, *J. Stat. Phys.* **52**:1119–1127 (1988).
8. S. Chen, K. Diemer, G. D. Doolen, K. Eggert, S. Gutman, and B. J. Travis, *Physica D* **47**:72 (1991).
9. S. Chen, Hudong Chen, Gary D. Doolen, S. Gutman, and M. Lee, *J. Stat. Phys.* **62**:1121 (1991).
10. S. Chen, G. D. Doolen, K. Eggert, D. Grunau, and E. Y. Loh, Lattice gas simulations of one and two-phase fluid flows using the connection machine-2, in *Proceeding of Discrete Models of Fluid Dynamics*, A. S. Aves, ed. (1991), p. 232.
11. D. Montgomery and G. D. Doolen, *Phys. Lett. A* **120**:229–231 (1987).
12. D. Montgomery and G. D. Doolen, *Complex Systems* **1**:831–838 (1987).
13. H. Chen and W. H. Matthaeus, *Phys. Rev. Lett.* **58**:1845 (1987).
14. H. Chen, W. H. Matthaeus, and L. W. Klein, *Phys. Fluids* **31**:1439–1445 (1988).
15. S. A. Orszag and V. Yakhot, *Phys. Rev. Lett.* **56**:1691–1693 (1986).
16. L. Kadanoff, G. McNamara, and G. Zanetti, *Phys. Rev. A* **40**:4527–4541 (1989).
17. S. Chen, Zhen-su She, L. C. Harrison, and G. D. Doolen, *Phys. Rev. A* **39**:2725–2727 (1989).
18. S. Chen, H. Chen, G. Doolen, Y. C. Lee, H. Rose, and H. Brand, *Physics D* **47**:97 (1991).
19. S. Chen, H. Chen, D. Martinéz, and W. Matthaeus, Lattice Boltzmann model for simulation of magnetohydrodynamics, *Phys. Rev. Lett.* (1992).